1

Introduction

1.1 Development and Practical Application of Single-crystal Nickel Alloy

Nickel alloys possess excellent comprehensive properties, such as high-temperature strength, high oxidation resistance, high fatigue resistance, and high thermal stability, and therefore have been employed widely in manufacturing the hot-end components of aeroengines [1, 2]. The development of nickel alloys goes through three generations, e.g., wrought nickel alloy, solidified directionally nickel alloy, and single-crystal nickel alloy (Figure 1.1). The temperature capability is enhanced from generation to generation. For example, compared to directionally solidified nickel alloy, a single-crystal turbine blade allows an operating temperature higher by around 25–50 °C, equivalent to an increase in turbine blade service life by up to 3 times from the aspect of working efficiency.

The turbine inlet temperature has been improved significantly for advanced aeroengines. Using the single-crystal hollow turbine blades can make the turbine inlet temperature reach 2100 K for the F119 aeroengine. At such a high temperature, the polycrystalline turbine blade formed by the conventional casting method can melt and cease to work. However, single-crystal turbine blade works well and is becoming the preferred choice of first-stage turbine blades of aeroengines with a higher thrust-weight ratio of above 10. This is mainly because the whole turbine blade grows from a single grain without any grain boundaries, which often induce defects of micropores and microcracks in polycrystalline nickel alloy (Figure 1.2). Meantime, the elements enhancing grain boundaries as well as decreasing the metal melting point can be reduced effectively (Figure 1.3). Thus, these promote the high temperature resistance of single-crystal nickel alloy. By using the advanced material preparation technique for single-crystal nickel alloy and the double-wall air cooling/casting-in-chill manufacturing technique for single-crystal turbine blade, the turbine inlet temperature can be increased to 2200 K, which makes the extreme machining of single-crystal nickel alloy one of the cutting-edge research topics in fabricating the military and commercial aeroengines.

Grinding of Single-crystal Superalloys: Fundamentals and Technologies, First Edition.
Wenfeng Ding et al.

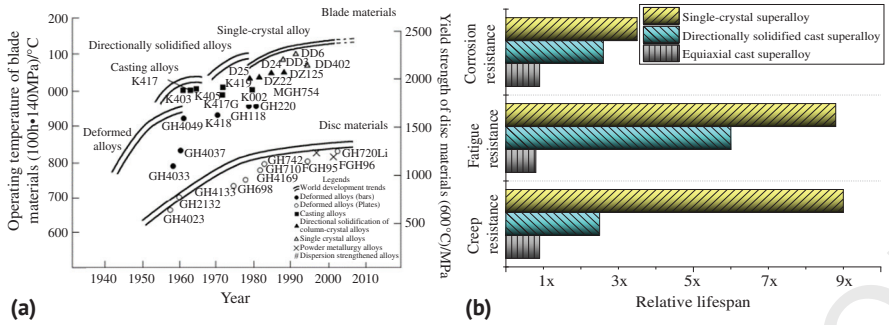

Figure 1.1 Development of (a) temperature capability and (b) mechanical properties of nickel alloys.

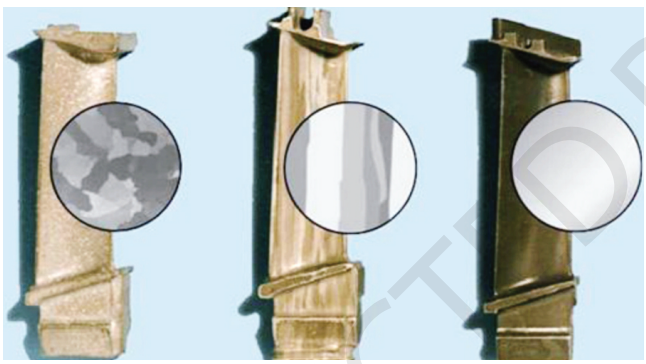

Figure 1.2 Microstructures in different casting nickel alloys: (a) equiaxial cast; (b) directionally solidified cast; and (c) single crystal [2]/Journal of Mechanical Engineering.

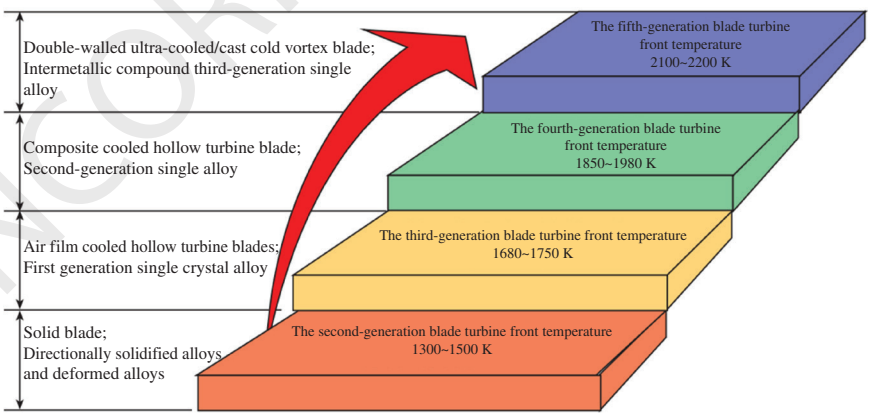

Figure 1.3 Application of single-crystal turbine blades in an advanced aeroengine. Adapted from [3].

1.2 Advantages of Grinding Technology of Single-crystal Nickel Alloy

Relying on the micro-cutting behaviors of thousands of abrasive grains on the wheel surface, the grinding process can fabricate a high-quality surface with low surface roughness, compressive stresses, and high accuracy (Tables 1.1 and 1.2), regardless of workpiece materials. This nature is different from the conventional turning, broaching, and milling methods, which often face major challenges in difficult-to-cut materials (i.e., nickel alloys) because of the rapid tool wear and the huge difficulty in controlling surface integrity and accuracy (Table 1.3). Currently, various grinding techniques have been developed to fulfill the requirements of different practical applications for almost any workpiece material (e.g., nickel alloys and ceramics). For instance, surface grinding is usually employed in manufacturing the automobile components and machine tools with flat surface requirements; profile grinding is usually combined with the creep-feed deep machining method that permits high efficiency in grinding the aeroengine parts with large stock removals and complex shapes; and micro grinding works as one of the effective methods to fabricate the micro features in metals. The common characteristic of the abovementioned grinding techniques is that the grinding process always serves as the final process to guarantee the workpiece surface quality.

In the case of aeroengine manufacturing, the typical features of nickel alloy turbine blades include high machining accuracy, good surface quality, and high fatigue resistance. Though the nontraditional machining methods (e.g., electrochemical

Table 1.1 Material removal rates achieved in the common grinding process.

Contents	Shallow grinding	Creep-feed grinding	High-speed grinding	High-efficiency deep grinding
Grinding depth a_p (mm)	Low 0.001–0.05	High 0.1–30	Low 0.003–0.05	High 0.1–30
Workpiece speed v_w (m/min)	High 1–15	Low 0.05–0.5	High 1–15	High 0.5–10
Grinding speed v_s (m/s)	Low 15–40	Low 15–40	High 60–200	High 60–200
Material removal rate Q_w' ($mm^3/(mm \cdot s)$)	Low 0.05–2	Low 1–10	Medium ≤ 60	High 50–2000

Table 1.2 Surface roughness achieved in the common grinding process.

Grinding methods	Conventional grinding	Precision grinding	Ultraprecision grinding	Mirror grinding
Surface roughness R_a (μm)	0.16–1.25	0.04–0.16	0.01–0.04	≤ 0.01

Table 1.3 Main methods and related characteristics for machining single-crystal nickel alloy components.

Machining method	Machining efficiency	Machining accuracy	Machined surface quality	Other characteristics
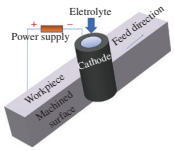 Electrochemical machining (ECM)	High	±50 μm	$R_a \leq 1.6$ μm, with slight/without affected layer	With slight/without electrode wear, suitable for mass production, large initial investment, and not environmentally friendly
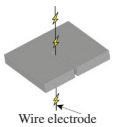 Electrical discharge machining (EDM)	Medium	±5 μm	$0.2 \leq R_a \leq 3.2$ μm, with affected layer and even microcrack	Suitable for any workpiece materials, having electrode wear, suitable for mass production, large initial investment, and not environmentally friendly
 Additive manufacturing	Low	±350 μm	$3.2 \leq R_a \leq 12.5$ μm, easy to deform	Limited workpiece size, difficulty in fixturing and supporting workpiece, and large initial investment
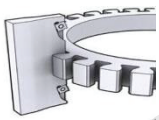 Broaching	Medium	≤ 10 μm	$0.8 \leq R_a \leq 1.6$ μm	Rapid tool wear and high cost
 Milling	Low	≤ 10 μm	$0.4 \leq R_a \leq 3.2$ μm	Rapid tool wear, limited workpiece size, and low machining efficiency
 Grinding	Medium	≤ 5 μm	$R_a \leq 0.6$ μm, with compressive stresses	Rapid tool wear if using conventional abrasive wheels, good surface quality

machining [ECM] and electrical discharge machining [EDM]) have achieved rapid developments in the past decades, the extremely strict requirements of tight tolerance (< 10 μm), low surface roughness (R_a < 0.6 μm), and high surface integrity still make the grinding process, particularly the profile grinding, dominate the main positions in machining aeroengine components. Therefore, both conventional grinding (including surface grinding and profile grinding) and micro-grinding are still attracting great attention in machining difficult-to-cut materials, especially single-crystal nickel alloys, and deserve further exploration.

1.3 High-efficiency Grinding Technology Development of Single-crystal Nickel Alloy

1.3.1 High-efficiency Grinding Mechanism and Development

During grinding, the workpiece material is removed in the form of tiny wedge-shaped chips by the effective cutting behavior of an individual abrasive grain. In the grinding zone, the interaction between abrasive grain and workpiece is complicated and always changing due to the varied penetration depth of abrasive grain into the workpiece. Thus, the grinding chip formation can be divided into three stages (Figure 1.4): (i) sliding, (ii) plowing, and (iii) cutting. The cutting stage is expected to be induced because of its effective material removal behavior. The other two states are expected to be avoided owing to their low efficiency in removing workpiece material, together with high grinding energy consumption. However, for each kind of workpiece material, the duration time of such three stages might be different even under identical grinding conditions. Understanding the underlying material removal mechanism of each workpiece material is essential to optimize the grinding process.

Furthermore, in surface grinding, the grinding loads are distributed uniformly along the grinding surface, and thus, the formation of surface integrity is relatively easy to clarify. Nevertheless, in profile grinding, there are various factors that limit the improvement of machining accuracy and surface quality, such as the long,

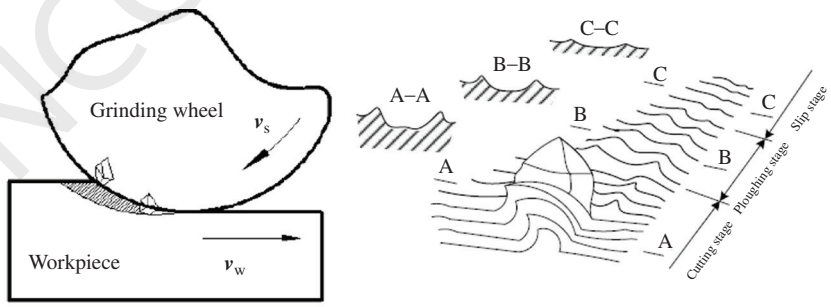

Figure 1.4 Schematic illustration of the material removal process in the grinding process.

narrow, and large contact zone, the complex workpiece shape, the varied grinding loads along workpiece shape, the insufficient and uneven cooling, the varied grinding wheel wear, etc. Jin et al. [4, 5] pointed out that by combining the theoretical model, experimental testing, and simulation method, the material removal process in profile grinding can be further understood. Because of the low thermal coefficient and high temperature strength, the grinding of nickel alloys often produces a large amount of grinding heat, which is distributed ununiformly (Figure 1.5) in the grinding zone. In other words, the strongly coupled thermo-mechanical-structural effects induce easily local grinding burn and microcracks on the workpiece surface.

To further improve the grinding efficiency, many scholars are dedicated to developing new ideas according to the classical formula of the maximum undeformed chip thickness of a single grain (Eq. 1-1).

$$a_{\mathrm{gmax}} = \left[\frac{4}{C \cdot N_{\mathrm{d}}} \cdot \frac{v_{\mathrm{w}}}{v_{\mathrm{s}}} \cdot \left(\frac{\mathrm{a_p}}{d_{\mathrm{s}}}\right)^{\frac{1}{2}}\right]^{\frac{1}{2}} \tag{1.1}$$

where a_{gmax} is the maximum undeformed chip thickness of a single grain, N_{d} is the active grain number, C is a constant related to grain edge, and d_{s}, a_{p}, v_{w}, and v_{s} are grinding wheel diameter, grinding depth, workpiece speed, and grinding speed.

Based on the above idea, creep-feed grinding process (CFDG) was developed in the 1950s, whose typical features are using large-porosity conventional abrasive grinding wheels, large grinding depths, and small workpiece speeds. This method can keep a small value of a_{gmax}, while improving the grinding efficiency remarkably and simultaneously maintaining the high surface quality. However, the sudden burning during grinding hinders the application of the creep-feed grinding method until Andrew et al. proposed the famous theory of film boiling and nucleate boiling of the grinding zone in the 1960s [6]. The problem of sudden burning is being overcome to some extent, promoting CFDG, which is widely employed in machining nickel alloys.

Recently, because of the improvement in the material properties of silicon carbide, alumina, cubic boron nitride (CBN), and diamond abrasive grains, various new grinding techniques (i.e., high-speed grinding, ultrahigh-speed grinding,

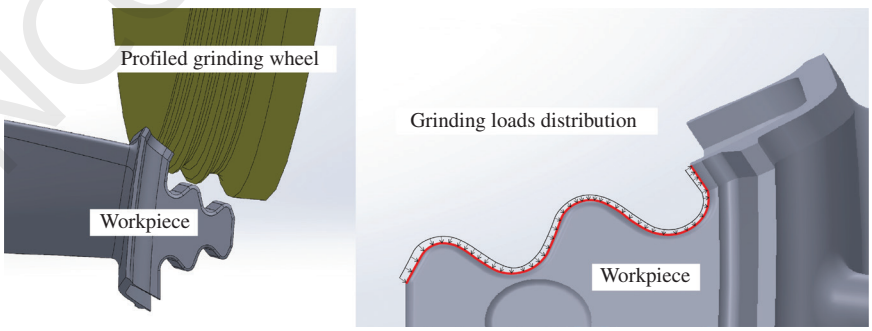

Figure 1.5 Schematic illustration of grinding loads along the turbine blade root shape.

high-efficiency deep grinding, composite energy-assisted grinding, and continuous dressing grinding) are developing vigorously [7, 8] (Figures 1.6 and 1.7). These provide effective methods to improve the grinding performance of abrasive wheels and the grindability of difficult-to-cut materials. However, the studies on such aspects are insufficient, such as the material removal mechanism, the process stability and adaptability, the formation and control mechanism of grinding surface integrity, the relationship between subsurface structure and mechanical properties at multi-scale size, etc. There still exists a big gap between practical application and laboratory study.

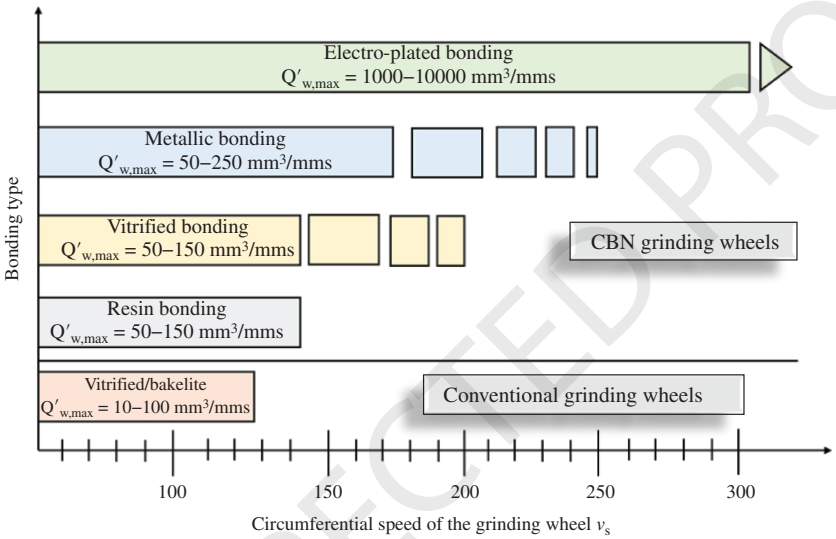

Figure 1.6 Development of abrasive grinding wheels.

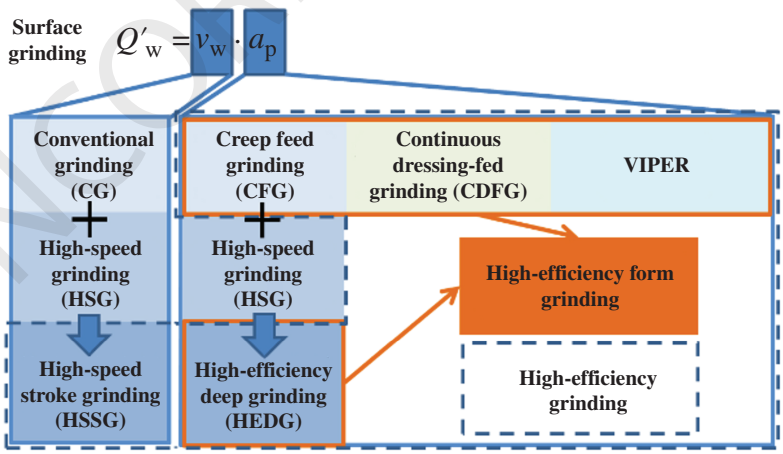

Figure 1.7 Development of grinding techniques.

1.3.2 High-efficiency Grinding Characteristics and Challenges

Numerous investigations have been conducted on the grindability of nickel alloys in the past decades. The related research contents can be as follows: (i) A series of advanced grinding machine tools and process parameters are developed, as well as various methods to improve the grinding performance of abrasive wheels, material removal rates (MRRs), and surface integrity of nickel alloys. (ii) The influencing factors on the grindability of nickel alloys are clarified (Figure 1.8), including the workpiece material properties, cooling behavior, machine performance, tool specification, dressing parameters, and grinding parameters. In particular, the challenges concerning low grinding efficiency, difficulty in controlling grinding burn, and insufficient understanding of micro-/nano-scaled surface integrity in nickel alloys are prominent. These are the main bottlenecks that restrict the realization of high-quality and high-efficiency grinding of nickel alloys and therefore become one of the cutting-edge research points in extreme manufacturing fields.

1. Low grinding efficiency

   Low grinding efficiency is one of the main problems in the grinding of nickel alloys. In general, the grinding efficiency is highly dependent on MRR, and MRR is decided by workpiece speed and grinding depth. Obviously, the tool wear and grinding surface quality play an important role in extending the grinding parameters.

   For wrought superalloys, a complete evaluation of the effects of grinding parameters, i.e., grinding speed v_s, workpiece speed v_w, and grinding depth a_p, on the machined surface integrity of Inconel 718 alloy was performed by Zeng et al. [9]. It was found that the machined surface integrity was highly sensitive to the grinding depth. If a small grinding depth was employed, the residual stress, microhardness, and microstructure alternations in ground surface layer could be much more localized. The optimized parameters were finally determined as $v_s = 20$ m/s, $v_w = 22$ m/min, $a_p = 0.015$ mm. Yao et al. [10] conducted a further

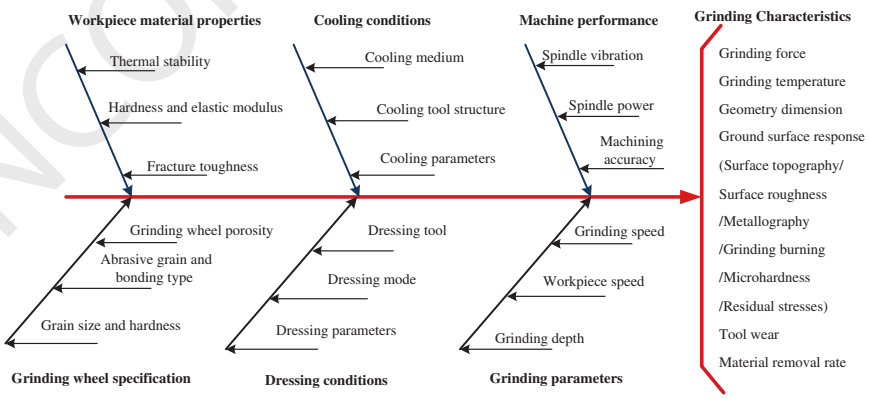

Figure 1.8 Fishbone diagram of influencing factors on grindability of nickel alloys.

investigation on the surface grinding of Inconel 718 alloy by using alumina wheels. The surface roughness of $R_a = 0.11$ μm, the softened ground surface layer of 30 − 40 μm, and the plastic deformation layer of 10 − 15 μm were identified when the MRR reached 1.3 $mm^3/(mm \cdot s)$ ($v_s = 25$ m/s, $v_w = 16$ m/min, $a_p = 0.005$ mm). At an MRR of 3.7 $mm^3/(mm \cdot s)$ ($v_s = 20$ m/s, $v_w = 15$ m/min, $a_p = 0.015$ mm), it was found that the chemical reactions between the abrasive grains and workpiece material led to strong workpiece material adhesion on the machined surface and the sharply increasing grinding force.

In the case of cast superalloys, Xu et al. [11–14] presented detailed studies on the grinding temperature and the tool wear mechanism, and their effects on surface integrity parameters in grinding of K417 alloy. Their observations indicated a clear effect of grinding temperature on the color evolution of the machined surface and on the microstructure evolution of the machined surface layer. The increasing ductile deformation of the workpiece was found to contribute to the chemical bonding between the abrasive grains and the workpiece at the elevated temperatures. Furthermore, Österle and Li [15] studied the subsurface microstructural changes of workpiece in creep-feed grinding of IN738LC alloy by using alumina wheels. Analysis of the microstructure evolution of workpiece cross section denoted the presence of local melting at contact spots that led to the formation of white layer when the MRR was 8 $mm^3/(mm \cdot s)$ ($v_s = 20$ m/s, $v_w = 0.48$ m/min, $a_p = 1$ mm). Chen et al. [16, 17] explored the grinding characteristics of DZ4 alloy using the MRR ranging from 0.24 to 3.75 $mm^3/(mm \cdot s)$. It was observed that the machined surface hardness was weakened remarkably by 25% and the depth of the affected layer exceeded 0.5 mm when the grinding temperature reached 1100 °C.

From the review of the aforementioned literature, the grindability upon different nickel-based superalloys using alumina wheels can be detailed in Table 1.4. It can be seen that the machined surface integrity and tool wear are influenced significantly by the grinding conditions and workpiece materials. Specifically, as more advanced superalloys are developed, i.e., from wrought to single-crystal nickel alloys, their comprehensive properties are further enhanced and improved. However, machining of such alloys becomes more difficult. High mechanical and thermal loads are usually associated with the grinding of nickel-based superalloys, leading to these undesirable features of machined surface (summarized in Table 1.4).

Furthermore, a practical result found in previous tests is that the rapid rate of wheel wear and low ability to maintain the dimensional accuracy are always the bottleneck for conventional abrasive wheels to reach a desired grinding efficiency. Increasing the dressing frequency tends to solve these practical problems, while the tool service life has to be greatly shortened. For this reason, the superhard abrasive wheels, e.g., CBN wheels, are proposed to be used for machining the fir-tree blade root, as reported by Zhao et al. [12], where a very high MRR of up to 50 $mm^3/(mm \cdot s)$ was achieved by using CBN wheels in the grinding of Inconel 718 alloy. Nevertheless, the high cost

Table 1.4 Grinding behavior of nickel alloys using conventional wheels.

Workpieces	MRR ($mm^3/(mm \cdot s)$)	Grinding parameters	Grinding wheel and its wear behavior	Ground surface integrity	References
Inconel718	6.67	$v_s = 25$ m/s, $v_w = 10$ m/min, $a_p = 0.04$ mm	Single Al_2O_3(80#)	$R_a = 0.89$ μm, surface crack	[9]
Inconel718	3.75	$v_s = 20$ m/s, $v_w = 15$ m/min, $a_p = 0.015$ mm	White Al_2O_3 (60#), strong material adhesion	$R_a = 0.6$ μm, grinding burn and feed marks	—
Inconel718	6.67	$v_s = 25$ m/s, $v_w = 16$ m/min, $a_p = 0.025$ mm	Single Al_2O_3 (80#)	$R_a = 0.18$ μm, many feed marks	[10]
K417	1.40	$v_s = 25$ m/s, $v_w = 0.07$ m/min, $a_p = 1.2$ mm	White Al_2O_3 (100#), strong chemical bonding	$R_a = 1.2$ μm, grinding burn with puce color on ground surface and remarkable smeared materials	[11–14]
DZ4	3.75	$v_s = 25$ m/s, $v_w = 1.5$ m/min, $a_p = 0.15$ mm	White Al_2O_3 (60#)	Recrystallization near ground surface	[16, 17]
IN738LC	2.00	$v_s = 20$ m/s, $v_w = 0.12$ m/min, $a_p = 1$ mm	White Al_2O_3 (60#)	White layer and internal microcracks	[15]

and the low potential concerning the dressing capability are generally major problems for superhard abrasive wheels to profile grinding, even though it is demonstrated that the active surfaces of superhard abrasive wheels can be specially designed and textured, and are capable of creep-feed grinding deep fir-tree slots and fir-tree root forms in the difficult-to-cut nickel alloys with free workpiece burning. On the contrary, due to the low hardness and cost-effective price compared to the superhard abrasive wheels, conventional abrasive wheels are evidenced with an excellent profiling ability and have become widely applied in the turbine blade root manufacture. High surface quality, e.g., the surface roughness of R_a 0.65 μm and the compressive stress of up to 490 MPa, was achieved. Guo et al. [18, 19] developed the process to realize the continuous dressing creep-feed profile grinding of the fir-tree

blade root forms using conventional abrasive wheels. Control of the blade root grinding process was further optimized by monitoring the power signature and adjusting the dress infeed rate and workpiece speed to improve the grinding efficiency. The results of the above tests indicate that the relatively short service life of conventional abrasive wheels can be offset by high profiling ability and acceptable surface quality.

In addition, the newly developed microcrystalline alumina abrasive wheels have a higher potential for profile grinding as evidenced by the large grinding ratios, high MRRs, low grinding forces, low geometrical wear, and good ground surface integrity compared to the conventional abrasive wheels. This type of grinding wheel is therefore very suitable for creep-feed profile grinding blade root forms though further investigations have to be done to optimize the process results. Note that the best option for grinding of nickel alloys can be determined usually by comprehensively considering the machining cost, machined surface quality, and machining complexity. Therefore, it is still of utmost importance to study grinding techniques to further improve the grinding efficiency of nickel alloys.

2. Difficult controlling of grinding burn

Grinding burn is induced by massive heat accumulation in the grinding zone and usually leads to a very high temperature together with the alternation of appearance and microstructure of workpiece surface layer. As mentioned earlier, the high grinding force and temperature can be generated even though a small MRR is used for grinding with alumina wheels. Under such conditions, grinding burn is difficult to control. Moreover, the poor cooling effectiveness or/and severe wheel wear could also result in the occurrence of grinding burn with an instantaneous temperature of more than 1000 °C (Figure 1.9). Grinding burn limits the improvement of grinding efficiency significantly and is deleterious to the grinding surface integrity. Because of the sensitivity of single-crystal nickel alloy in aeroengine field, the components must be scrapped even if a slight grinding burn occurs. Thus, it is necessary to avoid the grinding burn through the detection and prediction methods.

Figure 1.9 Typical grinding burn on fir-tree turbine blade root surface.

Almost all indicators of surface integrity are affected by grinding burn. At present, the identification of grinding burn is performed mainly by the response features of the ground surface/subsurface, such as surface topography and appearance, microstructure, microhardness, and noise detection. In addition, the monitoring of sudden changes in grinding force, temperature, and grinding power can also be used to identify the grinding burn. An effective and early warning of grinding burn is of significant importance to ensure the grinding quality and save the economic loss due to scrapped components.

It is notable that the grinding temperature is critical to monitor grinding burn. To prevent the workpiece from burning, the theoretical and simulated models should be developed to figure out the evolution and distribution of temperature under typical grinding conditions (Figure 1.10). Then the thermal-induced surface/subsurface damage can be predicted, which can provide useful guidance for the process design in the following grinding arrangements. Although the possibility of achieving the dimensional tolerance of less than 10 μm and surface roughness R_a of less than 0.6 μm has been reported in creep-feed grinding (CFG), diverse thermal damage has still been reported as the biggest issue, including large tensile residual stress, thermal softening, burns, and microcracks. Although substantial efforts were made to understand grinding temperature even with the consideration of stochastic nature, the high temperature in CFG of blade roots seemed to be different due to the limited coolant transportation in the grinding zone, the very high specific energy in CFG, and the low thermal conductivity of nickel-based superalloys [20]. To gain a more in-depth understanding, multitudes of efforts and attentions from both academic and engineering aspects have already been made, and most of them can be categorized into two groups: (i) theoretical and (ii) numerical studies.

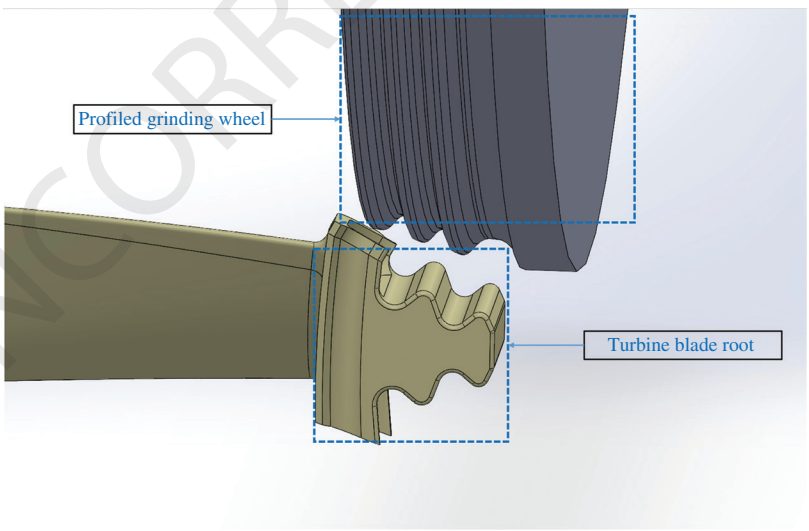

Figure 1.10 Grinding of the fir tree-shaped/profile of turbine blade root.

For the theoretical aspect, the pioneer work started with the one-dimensional (1D) analytical modelling of the heat transfer within the grinding zone where the maximum temperature in CFG considering the grinding fluids was modeled and the critical temperature for film boiling to occur in the grinding zone was determined on the basis of the analytical results. Guo and Malkin [19] further developed the model so as to predict the critical heat flux for burns in CFG, and the energy partition in CFG was estimated as 4.5% for up grinding and 3% for down grinding during certain conditions. The best match between theoretical and experimental results was found when using the heat source with the scalene-triangular-shaped heat flux, and the energy partition to the workpiece was found to be 4.3% for up CFG and 3.5% for down CFG. Except for all the above studies focusing on the CFG process of flat surfaces, Jin et al. [21, 22] presented the three-dimensional (3D) analytical model in creep-feed grinding of curved surfaces of gears. The effect of the contact geometry along the gear tooth profile on the grinding temperature distribution was analyzed while taking into account gear teeth number, module, and rolling angle. The heat source with the triangular-shaped heat flux was used to calculate the temperature profiles, and the simulated results indicated a good agreement with the measured temperature, with the maximum relative error being only 10.3%. The more comprehensive 3D grinding temperature model can be the stochastically grain-discretized temperature model, where the grain-workpiece micro-interactions (including rubbing, plowing, and cutting) and the corresponding varied thermal effects were considered. The relative difference between the calculated and experimental results of less than 20% was reported, proving the model's accuracy to a large extent. More importantly, both the two-dimensional (2D) and 3D grinding temperature domains with highly localized details at the grain scale were obtained for the first time. More details about theoretical grinding temperature work can also be found in Refs. [23] and [24].

Parallel to the theoretical studies, extensive numerical studies on the grinding temperature were also carried out based on finite element method (FEM) due to their good visualization and powerful ability to solve multiphysics problems. The 2D simulation results were found to be generally consistent with the experimental ones, with the relative error of less than 20%. The detailed effects of various grinding parameters (e.g., wheel speed, workpiece feed rate, grinding depth, and fluid properties) on the temperature distribution were investigated comparatively based on the 2D finite element (FE) model with a rectangular heat source. The simulated results matched the experimental data where an error of around 10% was found. The effect of dynamic viscosity and surface tension of the grinding fluid on the grinding temperature domain was found to be much more significant than that of the specific heat capacity of grinding fluids. The obtained results were consistent with the reports from Jin [5], indicating the parabolic heat source might be more suitable to estimate grinding temperature in the high-efficiency deep grinding due to the high geometrical similarity of the workpiece–wheel contact zone to the parabolic surface.

With the availability of the aforementioned studies, it might be noted that very few studies focus on the temperature modelling in the CFG of single-crystal

turbine blade roots where the workpiece–wheel contact region has a relatively complex profile. The non-flat workpiece–wheel contact zone might make the temperature field even more complicated due to the temperature concentration, thanks to the lack of heat convection. Therefore, in practice, the factories for manufacturing the aeroengine components take mild process parameters to grind the nickel alloys in order to ensure a burn-free grinding surface. In addition, the grinding wheels are dressed frequently to maintain the sharpness and shape accuracy. This operation inevitably decreases the grinding efficiency. As a result, there exist great challenges to obtain the desirable surface integrity of nickel alloys as well as the high geometry accuracy of the workpiece.

3. Insufficient understanding of micro-/nano-scaled surface integrity
Due to the complex thermo-mechanical interaction between grinding tools and workpiece, severe plastic deformation (SPD) always takes place in the superficial layer of workpieces, usually leading to local alterations of microstructure (e.g., grain refinement) and material properties (e.g., work hardening) (Figure 1.11). Understanding these alterations and the underlying formation mechanism has been a prominent topic in previous studies, because of their significant effects on surface integrity, which determines the fatigue life, creep, fracture, and tribological properties of nickel-based superalloy components [14]. However, because of the difficulty in detection methods and the lack of analytical knowledge, the studies on micro-/nano-scaled surface integrity are insufficient.

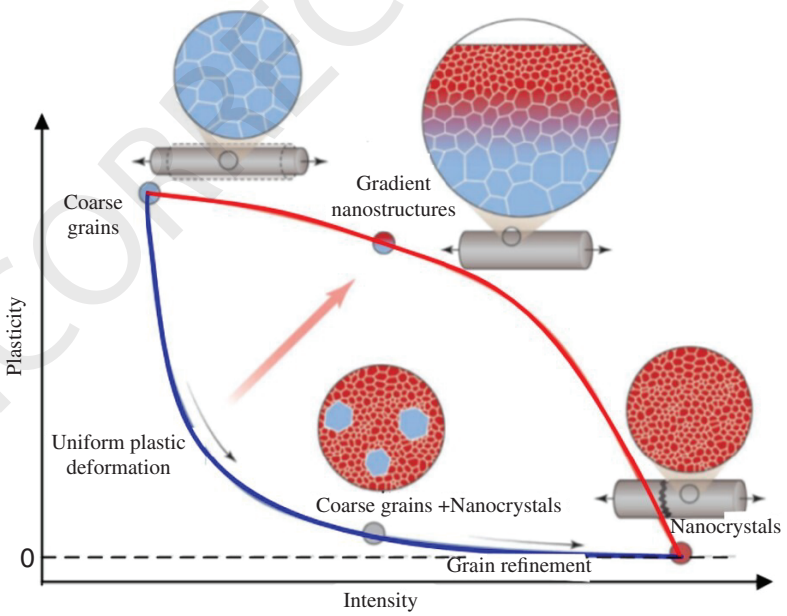

Figure 1.11 Relationship between mechanical properties and microstructures.

For this reason, numerical investigations are dedicated to clarifying the effects of mechanical grinding on the workpiece microstructure and material properties at the micro- and nano-scale. For example, Ding et al. [25] examined the subsurface metallurgical alteration of the ground groove of K424 cast nickel-based superalloy produced by creep-feed grinding. Crystal lattice composed of the γ, γ', and γ'' phases was observed with moderate plastic deformation and distortion (up to 30 μm in thickness). High work hardening (up to 46% above the bulk hardness) was found in the workpiece superficial layer. This change in microstructure of nickel-based superalloys is owing to the high thermal energy and high mechanical deformation during grinding, whose competing influence determines the transition between hardening and softening in material properties. Furthermore, under a given machining condition, the white layer, which exhibits featureless and white appearance using an optical microscope, can be formed in the machined surface. It is usually detrimental to the fatigue life of the machined workpiece because of its hard and brittle nature. A full exploration on such a white layer was conducted by Liao et al. [26] who studied in detail the formation mechanism, microstructure, and mechanical properties of the white layer of S135H nickel-based superalloy. It was indicated that the deterioration of the white layer to material properties was attributed to the dissolution of γ' strengthening phase, although the grain refinement, which was beneficial for improving material performance to some extent, can be obtained within the white layer.

However, it is worth underlining that the mechanical grinding has been proved as an effective way to modify the material properties by introducing refined grains to the workpiece surface. As presented by Ding et al. [27–29], a gradient microstructure (i.e., surface nano-laminated structure, deformation-twinned structure, and severely deformed structure) of Hastelloy C-22HS nickel-based superalloy could be produced by mechanical grinding. By virtue of micro-pillar compression tests, the yield strength of about 1650 MPa for both nano-laminated structure and deformation-twinned structure was achieved, which was greater by around 3.7 times than that of the bulk material. In addition, Liu et al. [22] reported an ultrahard and ultrastable nano-laminated structure (about 6.4 GPa at 504 °C) induced by high-rate shear deformation during grinding of polycrystalline nickel alloy. It was further found that the dislocation activities determined the formation mechanism of such a special structure.

Interestingly, it can be found in the above analysis that mechanical grinding, on one hand, can enhance material properties through grain refinement, but on the other hand, it can degrade the service performance of the workpiece under high temperature and stress conditions by inducing local detrimental modifications. For such a paradox, a deep understanding is of utmost importance for controlling material properties through grain refinement due to mechanical grinding.

It is noted that the single-crystal nickel-based superalloy grows from one single grain and eliminates the grain boundaries thoroughly. Therefore, it is capable of withstanding higher thermal and mechanical loads than the

polycrystalline one. This makes them one of the key materials used for the manufacture of turbine blade root, which works under extremely high temperature and pressure. However, such a single-crystal alloy is very sensitive to the stress concentration during mechanical grinding. Up to now, great efforts have been devoted to purposely achieve some special structures via mechanical grinding, which could allow for the tailoring of high-temperature performance of polycrystalline nickel-based superalloys [30, 31]. Nevertheless, the studies for the grinding-induced surface alterations have rarely been reported for the single-crystal nickel-based superalloy. Hence, questions are raised about how the grinding-induced surface alteration behaves in the microstructure, and whether the mechanical grinding could introduce a beneficial impact on the material performance via grain refinement; the answers are still not clear for the single-crystal nickel-based superalloys. As a consequence, it is urgent to conduct an investigation into the micro-/nano-scaled surface integrity of single-crystal nickel alloys in the grinding process.

1.4 Micro-grinding Technology Development of Single-crystal Nickel Alloy

1.4.1 Micro-grinding Mechanism of Single-crystal Nickel Alloy

With the rapid development of industries such as aerospace, defense, bioengineering, modern medicine, and microelectronics, the demand for 3D micro-components ranging from micrometers to millimeters, with high precision in size and surface quality, is becoming increasingly urgent, including micro-optical elements and microsensors (Figure 1.12).

Currently, machining methods like micro-milling, photolithography, EDM, and laser processing can create microstructures such as micro-holes and microgrooves ranging from several micrometers to hundreds of micrometers. However, issues like edge burrs, thermal damage, and electrochemical corrosion layers on the surface/subsurface exist. These problems exacerbate the contradiction between

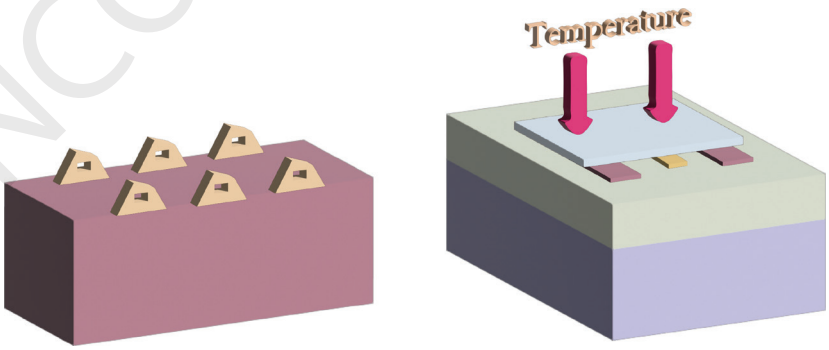

Figure 1.12 Microproducts and microstructures: (a) aerospace microproducts; (b) microsensors; (c) micro inertial switch; and (d) mirror processing.

machining quality, efficiency, and demands. Achieving high-quality, efficient machining of complex-shaped 3D micro-parts has become a pressing challenge in mechanical manufacturing.

At present, micro-grinding technology has drawn widespread attention from domestic and international researchers. However, research on micro-grinding tool design and preparation methods, micro-grinding mechanisms, and micro-grinding process equipment is still in the exploratory stage. A complete theoretical system and technical application capabilities have not been formed yet. Thus, research on improving the design, preparation, and processing technology of micro-grinding tools is of great theoretical and engineering application value. It can enrich the preparation methods of micro-grinding tools, extend their service life, and enhance the quality of micro-grinding processes.

Micro-grinding technology is a machining method that achieves micro-/nano-scale mechanical removal of workpiece surfaces using micro-sized grinding tools. It has a competitive edge over other fine mechanical machining technologies in obtaining 3D micro-parts and microstructures with high dimensional accuracy and surface quality.

The micro-grinding tools used in the micro-grinding process are mainly divided into ultrathin grinding blades (with a grinding part thickness of less than 1 mm) and micro-grinding rods (with a grinding part diameter less than 1 mm). Among them, cylindrical micro-grinding rods can perform micro-grinding on various complex microstructures and are the main micro-grinding tools [32].

The abrasive particles on the surface of the micro-grinding tool are very fine and closely distributed, resulting in limited chip accommodation space. Moreover, the chip size is close to the abrasive particle size, which easily causes chip clogging between the abrasive particles, leading to premature failure of the micro-grinding tool. Additionally, due to the small size of the micro-grinding tool, secondary dressing is difficult, severely affecting the surface quality of micro-grinding and the tool's service life. Therefore, the service life of existing micro-grinding tools has become one of the key factors restricting the widespread application of micro-grinding technology. Overall, research on micro-grinding mechanisms, processes, and tools is still in the exploratory stage, lacking a complete and mature technical system and manufacturing application capability.

Micro-grinding can achieve high machining precision and excellent surface quality for micro-components or microstructures through micro–nano mechanical material removal on the workpiece surface. This is accomplished using a micro-grinding tool embedded with ultrafine abrasive particle. Unlike conventional macroscale grinding, micro-grinding operates under different mechanisms.

The micro-abrasive tools used in micro-grinding are mainly classified into ultrathin grinding segments with a grinding section thickness of less than 1 mm and micro-abrasive rods with diameters under 1 mm. Given the significant reduction in the diameter of these micro-abrasive tools, factors typically ignored in conventional grinding, such as grinding wheel deformation and ploughing forces, become crucial and cannot be overlooked in micro-grinding. Furthermore, in micro-grinding, the depth of cut by abrasive grains is generally less than the particle size of the workpiece material. This situation leads to significant changes in the

material removal mechanism due to size effects and microstructural recrystallization phenomena [33].

Material micro-grinding processes macroscopically appear as the removal of workpiece material under the external force of the cutting tool, resulting in a machined surface and grinding debris. Microscopically, this process is characterized by irreversible permanent plastic deformation or even fracture of the workpiece material.

The fracture modes of polycrystalline metal materials include intragranular (within the grain) and intergranular (between grains) fractures. Under the external stress of abrasive particles, slip systems within the grains start and accumulate to form slip bands that extend toward the grain boundaries. Due to the orientation differences between adjacent grains, the primary slip initiation in one grain makes it difficult for adjacent grains to initiate their main slip, resulting in strengthening. This strengthening effect shows the interaction between grain boundaries and dislocations within the grain.

The short-range stress field at the grain boundaries of polycrystalline materials makes it difficult for lattice dislocations to enter or cross the grain boundary. The hindrance of grain boundaries to the movement of dislocations within the grains causes uneven and discontinuous deformation at the grain boundaries, leading to stress concentration. As the grinding process progresses, a large number of dislocations generated within the grains can be absorbed by the grain boundaries, releasing the corresponding stress concentrations. The accumulation of dislocations at the grain boundaries leads to grain boundary migration and fracture, thus forming grinding shear slip bands and grinding debris.

Unlike polycrystalline materials, single-crystal materials consist of a single grain without any grain boundaries. The atoms of nickel-based single-crystal superalloy are arranged periodically and repetitively in 3D space. The unit cell of the nickel-based single-crystal superalloy is shown in Figure 1.13a, with a face-centered cubic (FCC) structure. Figure 1.13b and c compare the 2D atomic arrangements of single-crystal and polycrystalline materials: the atomic arrangement in single-crystal materials forms a long-range ordered structure, while polycrystalline materials are composed of numerous grains with different atomic orientations. In Figure 1.13a, the black dots represent metal atoms, and the straight lines indicate the bonds between atoms.

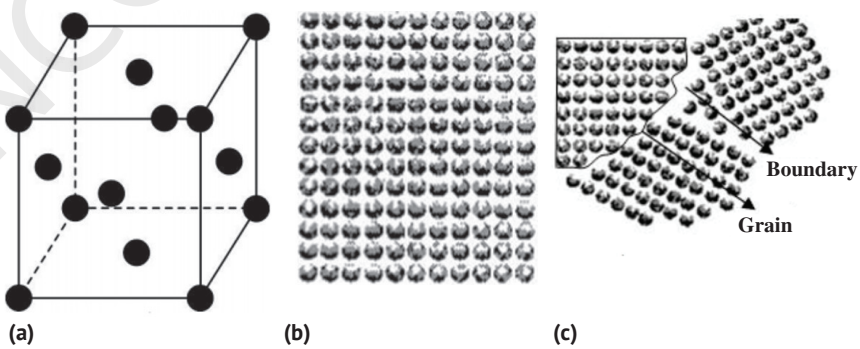

Figure 1.13 (a) Face-centered cubic lattice, and atomic arrangement of (b) single-crystal and (c) polycrystalline material.

Under the action of grinding force, dislocations are generated within the lattice of a single-crystal material, initiating slip. When internal slip and fracture occur within the lattice, they encounter various resistances. The most fundamental inherent resistance is the lattice resistance, commonly known as the Peierls stress, as shown in -Eq. 1.2. This resistance comes from the crystal lattice's hindrance to the movement of dislocations within the lattice, mainly due to the attractive forces between the atoms on the two layers corresponding to the slip plane.

$$\tau_p = \frac{2G}{1-v} e^{-\frac{2\pi m}{n(1-v)}} \tag{1.2}$$

where G represents the material's shear modulus, v is Poisson's ratio, m is the interplanar spacing, and n is the atomic spacing along the slip direction. Evidently, its magnitude is directly determined by interplanar spacing and atomic spacing. In a crystal, different crystallographic planes have different interplanar spacings. According to Eq. 1-2, the largest interplanar spacing corresponds to weaker atomic bonding forces between the planes, resulting in the smallest lattice resistance to slip, which often makes slip more likely to occur. The slip direction in a crystal is usually along the direction of close-packed atoms, and the interplanar spacing increases with the atomic density within the plane. Lattice dislocation slip first occurs in the direction of closely packed planes because the atomic bonding forces are stronger within high-density planes, making slip less likely, whereas the bonding forces between closely packed planes are weaker.

During the microscale grinding process, the nickel-based single-crystal superalloy DD98 undergoes slip and fracture on the (111) plane due to the shear forces of abrasive particles. The direction of slip is often along the most closely packed crystallographic orientation in the crystal. Figure 1.14 shows the various slip planes within the {111} family of lattice planes and their corresponding slip directions, including: the [101], [011], and [110] crystallographic directions within the (111) plane, as shown in Figure 1.14a; the [110], [011], and [101] crystallographic directions within the (111) plane, as shown in Figure 1.14b; the [101], [011], and [110] crystallographic directions within the (111) plane, as shown in Figure 1.14c; and the [110], [101], and [011] crystallographic directions within the (111) plane, as shown in Figure 1.14d.

The essence of nanomachining single-crystal nickel is to break the bonds between nickel atoms within the original single crystal, achieving atomic-level removal.

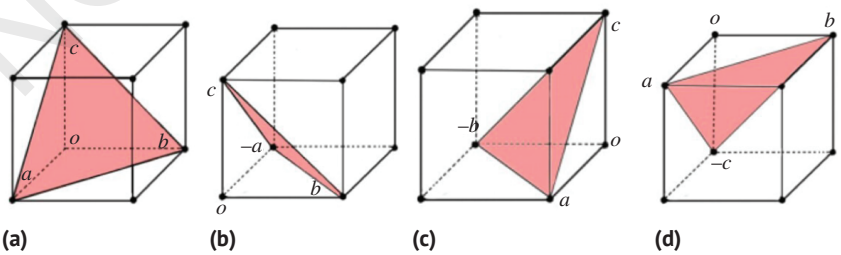

Figure 1.14 Gliding plane and direction of face-centered cubic lattice: (a) (111) plane; (b) $(\bar{1}11)$ plane; (c) $(1\bar{1}1)$ plane; and (d) $(11\bar{1})$ plane. Adapted from [4].

Therefore, during the machining process, the breaking of atomic bonds and the generation of defects should be considered as the starting point for studying material failure.

By using the atomic displacement vector method, one can track the magnitude and direction of each atom's displacement when the workpiece material deforms, allowing for a more direct observation of the flow direction and deformation extent of the material atoms. The displacement vectors of the defect atoms at machining distances of 0.4 nm and 0.7 nm are shown in Figure 1.15a and b [16], respectively, which show the displacement vectors of surface atoms corresponding to the above-mentioned machining distances.

As shown in Figure 1.15a, when the machining distance is 0.4 nm, the workpiece atoms in contact with the tool are compressed toward the interior of the workpiece by the tool. As the force at the contact point gradually increases, defect atoms gradually accumulate and form clusters of defect atoms. These atoms exhibit a displacement trend toward the [110] direction due to the breaking of atomic bonds. At this time, the displacement vector direction of the defect atoms is not on the slip plane of the single crystal. This is because, at the initial stage of machining, the slip system of the crystal has not yet been activated, and the displacement of defect atoms within the material has not yet reflected the characteristics of single-crystal materials.

Figure 1.15b shows the atomic displacement vector situation on the upper surface of the workpiece. It can be seen that under the pushing effect of the tool, the displacement change of surface atoms is relatively uniform, and the overall displacement decreases with the increase of the distance between surface atoms and the tool. Moreover, the displaced surface atoms only remain on the workpiece surface near the tool, indicating that the force acting on the workpiece is relatively concentrated. Furthermore, the displacement direction of surface atoms is consistent with the machining direction, and the displacement difference between adjacent atoms

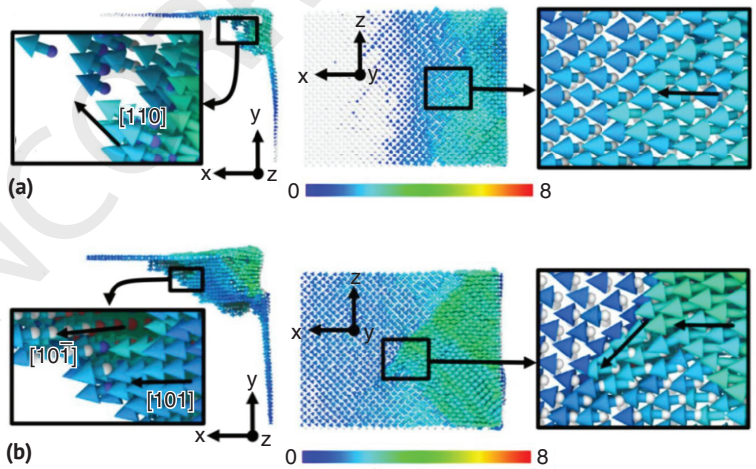

Figure 1.15 Defect atomic displacement vectors at cutting distances of (a) 0.4 nm and (b) 0.7 nm. Zhu et al., (2016)/Springer Nature.

is not significant, indicating that the workpiece surface has not yet experienced cracks or other forms of damage caused by machining.

In the micro–nano machining of single-crystal nickel, the process by which atoms in the machined part detach from the substrate is not a rigid slip on one side relative to the other as a whole, but rather it is achieved through the movement of dislocations. When a dislocation moves from within the material to the surface, it is equivalent to the entire region swept by its dislocation line having slipped one unit distance (the distance between adjacent lattice planes) along the direction of its Burgers vector. Thus, as dislocations continuously originate from within the material and move to the surface, they can provide the interplanar slip required for continuous plastic deformation.

In the micro–nano machining of single-crystal nickel, the process by which atoms in the machined part detach from the substrate is not a rigid slip on one side relative to the other as a whole, but rather it is achieved through the movement of dislocations. When a dislocation moves from within the material to the surface, it is equivalent to the entire region swept by its dislocation line having slipped one unit distance (the distance between adjacent lattice planes) along the direction of its Burgers vector. Thus, as dislocations continuously originate from within the material and move to the surface, they can provide the interplanar slip required for continuous plastic deformation.

The machining process of the crystal, as well as the conditions under which the crystal was formed and the thermal motion of atoms, has a direct impact on the generation of defects within the crystal. Moreover, crystal defects evolve continuously with changes in various conditions. The nucleation and movement of crystal defects are an important form of plastic deformation in metallic materials, and the machining process of the crystal is accompanied by the nucleation, movement, interaction, and annihilation of dislocations.

During the nanomachining process of single-crystal nickel, special defect structures may form due to the interaction between dislocations as they move within the crystal. The internal defect evolution within the workpiece is shown in Figure 1.16.

Figure 1.16a shows the defect situation when the machining distance is 4 nm. It can be seen that since the abrasive particles have not fully entered the workpiece, the entire machining process has not reached a stable state. At this time, many larger volume stacking faults extend into the interior of the workpiece.

As machining progresses, the primary shear zone forms a high-temperature and high-pressure region dominated by amorphous atoms. The high temperature reduces the nucleation energy for dislocations, leading to dislocation proliferation. Once dislocations nucleate, they do not immediately move away but instead swirl around in the shear zone. Two Shockley partial dislocations evolve on different slip planes within the crystal, meet, and hinder each other, forming an L-C dislocation lock. Dislocation climb occurs perpendicular to the original extension direction, and ladder dislocations form at the dislocation junction lines. This ladder dislocation, along with two partial dislocations, collectively forms a “V”-shaped dislocation loop, as shown in Figure 1.16b. Since the “V”-shaped dislocation loop is supported by the L-C dislocation lock, it has a certain stability.

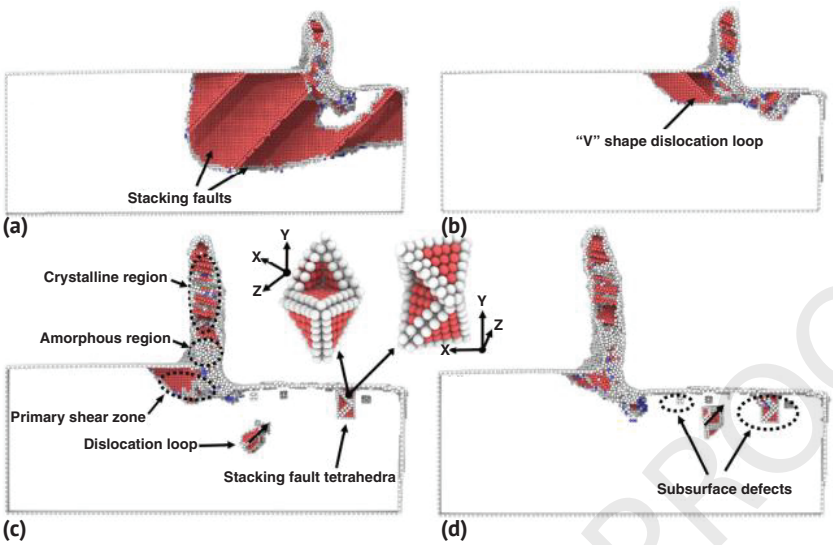

Figure 1.16 Snapshots of workpiece defects during nanometric machining at a machining speed of 200 m/s at different cutting distances of (a) 4.0, (b) 4.8, (c) 12, and (d) 15 nm.

From Figure 1.16c, it is evident that there is a clear layered phenomenon in the atom types in the upper part of the chip, the lower part, and the primary shear zone, mainly due to different forces and temperatures experienced by various regions during machining. Atoms entering different regions change into different structural types due to changes in external forces and temperatures.

Due to the extrusion effect of the rear tool face, dislocations nucleated below the tool inside the workpiece do not have enough energy to expand to the free surface and instead form closed dislocation loops within the workpiece, as shown in Figure 1.16c. When the tool leaves and the external force disappears, the stored energy inside the workpiece begins to release, causing the dislocation loops to move toward the machined surface and eventually disappear at the workpiece surface.

Due to the extrusion effect of the rear tool face, dislocations nucleated below the tool inside the workpiece do not have enough energy to expand to the free surface and instead form closed dislocation loops within the workpiece, as shown in Figure 1.16c. When the tool leaves and the external force disappears, the stored energy inside the workpiece begins to release, causing the dislocation loops to move toward the machined surface and eventually disappear at the workpiece surface.

In the micro-grinding process, material removal can be classified into three stages: rubbing, ploughing, and chip formation. Each stage corresponds to different surface generation mechanisms and exhibits different mechanical behaviors. The shape of the abrasive grit significantly influences the micro-grinding process.

During the rubbing stage (l_e), elastic and local plastic deformations are mainly governed by elastic forces acting on the workpiece. Some larger abrasive particles exceed the strength limit and form chips [34].

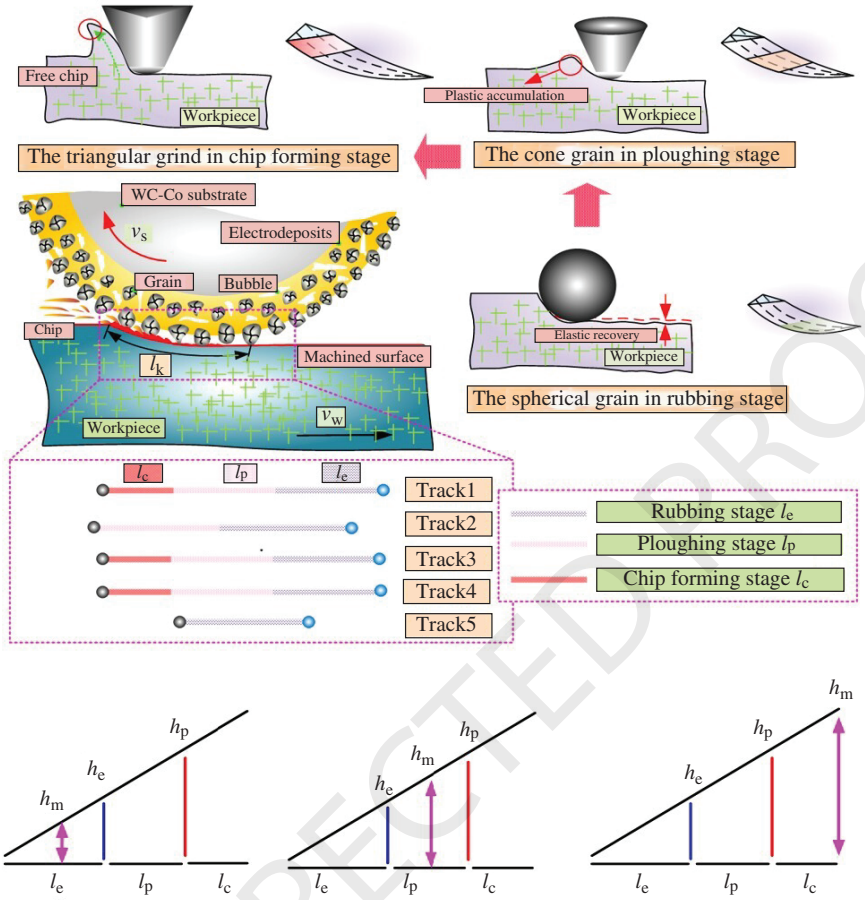

Figure 1.17 Schematic diagram of micro-grinding stage division for single-crystal superalloy.

The micro-grinding process of single-crystal superalloy material using the micro-grinding tool is illustrated in Figure 1.17. As the cutting depth increases, the contact effect between abrasive particles and workpiece continuously intensifies, eventually surpassing the yield strength and transitioning into the ploughing stage (l_p). In this stage, the number of abrasive particles forming chips rises compared to the rubbing stage, with material removal mainly manifested as plastic flow under the influence of cultivated pears.

With further increases in cutting depth, the micro-grinding force exerted by most abrasive grains surpasses the ultimate strength, ultimately leading to free chip formation and reaching the chip-forming stage (l_c). However, a small number of abrasive particles remain in the elastic contact stage.

The actual cutting depth of the abrasive grains differs from the grinding depth and is instead the undeformed chip thickness h_m, as shown in Figure 1.18. To calculate the undeformed chip thickness, it is necessary to know the interval between

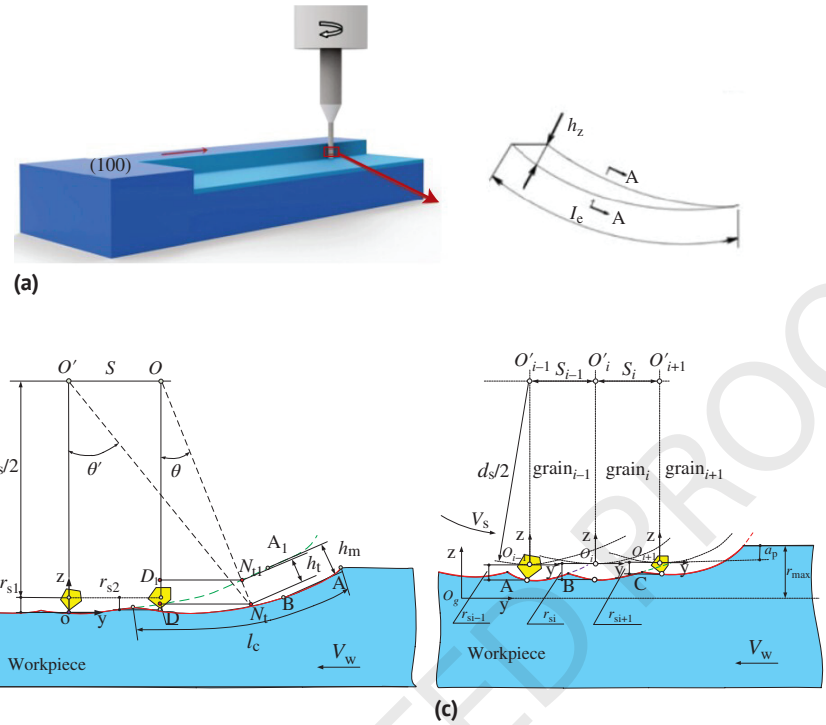

Figure 1.18 (a) Undeformed chip thickness and chip in surface grinding, and motion trajectories of (b) single abrasive particle and (c) multi-abrasive particles.

two consecutive cutting edges L, the number of cutting edges per unit wheel area C, the average effective cutting width per edge b_c, the contact arc length l_c, the average undeformed chip thickness h_a, the grinding depth a_p, the spindle speed v_s, the feed rate v_w, and the grinding rod diameter d_s. Contact arc length between grinding wheel and workpiece [112]:

$$l_c = \frac{d_s\theta}{2} = \frac{d_s \arccos\left(1 - \frac{2a_p}{d_s}\right)}{2} \tag{1.3}$$

In traditional macroscale grinding, $2a_p << d_s$. For microscale grinding, it is essential to account for the influence of size effects. The quantity of chips produced per unit of time during the grinding process of the rod is determined by the product of the volume of each chip and the MRR of the rod and the h_m can be obtained as:

$$h_m = \left[\frac{4}{Cr}\left(\frac{v_w}{v_s}\right)\left(\frac{a_p}{d_s}\right)^{\frac{1}{2}}\right]^{\frac{1}{2}} \tag{1.4}$$

In traditional conventional-size grinding, the diameter of micro-grinding rods is typically less than 1 mm, with some micrometer-level rods developed internationally.

In microscale grinding, the grinding mechanism significantly differs from that of conventional grinding. During the process, the contact arc length between the

grinding rod and the workpiece is reduced, often approaching the same order of magnitude as the maximum undeformed cutting thickness of the abrasive grains. Therefore, when modelling the maximum undeformed cutting thickness for micro-grinding, it is crucial to consider the influence of the size effect. In the micro-grinding process, where h_m is nearly equal to l_m, as illustrated in Figure 1.18, the maximum undeformed cutting thickness for microscale grinding is:

$$h_m = \frac{2a_p\nu_w}{KC \cdot \nu_s b_c d_s \arccos\left(1 - \frac{2a_p}{d_s}\right)} \tag{1.5}$$

1.4.2 Characteristics and Challenges of Micro-grinding Process

Micro-grinding achieves high machining accuracy and excellent surface quality for micro-parts or structures through micro–nano mechanical removal on the workpiece surface using micro-abrasive tools with ultrafine abrasive particles. These micro-abrasive tools are generally classified into ultrathin grinding discs with a grinding section thickness of less than 1 mm and micro-abrasive rods with diameters under 1 mm.

Due to the significant reduction in the diameter of these micro-abrasive tools, factors typically negligible in conventional grinding, such as grinding wheel deformation and ploughing forces, have a substantial impact on the micro-grinding process and cannot be ignored. Additionally, in micro-grinding, the grinding depth of the abrasive particles often falls below the grain size of the workpiece material, resulting in size effects and microstructure recrystallization that significantly alter the material removal mechanism. Consequently, the micro-grinding mechanism differs markedly from that of traditional grinding, as summarized in the comparison of conventional and micro-grinding in Table 1.5.

Therefore, the mechanisms underlying micro-grinding processes are markedly distinct from those of traditional grinding. The comparison of highlighting key differences and characteristics between conventional and micro-grinding processes is emphasized in Table 1.5.

Table 1.5 Comparisons of micro-grinding and conventional grinding processes.

Content	Conventional grinding	Micro-grinding
Ratio of grinding radius to grinding depth	50~100	0.1~1
Plough effect	Not significant	Significant (20–30%)
Front rake angle	Constant negative	Variable negative
Feed rate (v_w)	1~30 m/min	0.000045~0.18 m/min
Cutting speed (v_s)	20~60 m/s	0.018~6 m/s
Material removal rate	10^2~10^{-1} $mm^3/mm \cdot s$	10^{-1}~10^{-3} $mm^3/mm \cdot s$

Micro-grinding can produce micro-parts and components with high dimensional accuracy and surface quality. It is a common choice for final finishing and can handle a wide range of materials, including hard and brittle substances like glass and ceramics, which are difficult to machine by traditional cutting methods. Microscale grinding can yield excellent results and is an effective way to improve micromachining quality. It typically uses small-sized grinding tools and processes the workpiece at a specific linear speed via a high-speed spindle.

Compared to micro-milling, research on micro-grinding started relatively late. Despite growing interest and progress, it remains an area with limited research. Brittle materials, which are prone to fracture under mechanical stress, are often machined by grinding. Achieving a transition to a ductile mode of removal can significantly improve machining quality. The current research progress of various scholars on micro-grinding is as follows:

Cheng et al. [35] conducted micro-grinding experiments on soda-lime glass to explore the material removal mechanism in brittle materials. They proposed a predictive model for brittle material removal in micro-grinding, considering size effects and abrasive tool surface topography. Based on the undeformed chip thickness, they classified the removal mechanisms into ductile, ductile-brittle transition, and brittle removal. Chip-type experiments showed that the edge chipping length varies significantly with the undeformed chip thickness. Coolant was found to be essential for ductile removal in soda-lime glass micro-grinding. The critical chip thicknesses for ductile-brittle transitions were determined to be 2 and 5 nm, respectively, and this was validated through grinding force variations.

Park [36] studied the influence of material grain structure, integrating thermal-mechanical coupling and size effects, to develop an interaction model for single-abrasive-grain removal at the microscale. This model incorporated a heat-transfer analysis based on a moving heat source to predict micro-grinding forces. By combining plowing and friction effects, the model evaluated the thermal influences on micro-grinding forces. Experimental calibration of heat distribution in the workpiece, using thermocouples and analytical calculations, confirmed the model's accuracy. Sensitivity analysis highlighted micro-grinding wheel and grain size as key influencing factors.

Wen et al. [32] systematically investigated the thermal characteristics of micro-grinding forces, surface roughness, and tool wear using electroplated micro-grinding tools. They established a mathematical model relating grinding forces to surface roughness and validated it against experimental data. FE simulations and thermocouple methods were used to analyze the workpiece temperature distribution during micro-grinding. Incorporating factors such as the minimum chip thickness and size effect, they created a model for the microscopic wear of grinding grains and studied the relationship between tool wear and workpiece surface roughness.

To improve micro-grinding performance, researchers have incorporated ultrasonic vibration-assisted technology into micro-grinding processes. Zhang et al. [18] conducted theoretical and experimental studies on ultrasonic vibration-assisted face micro-grinding. They developed a theoretical model based on how ultrasonic vibration geometry affects the instantaneous cutting thickness of abrasive grains.

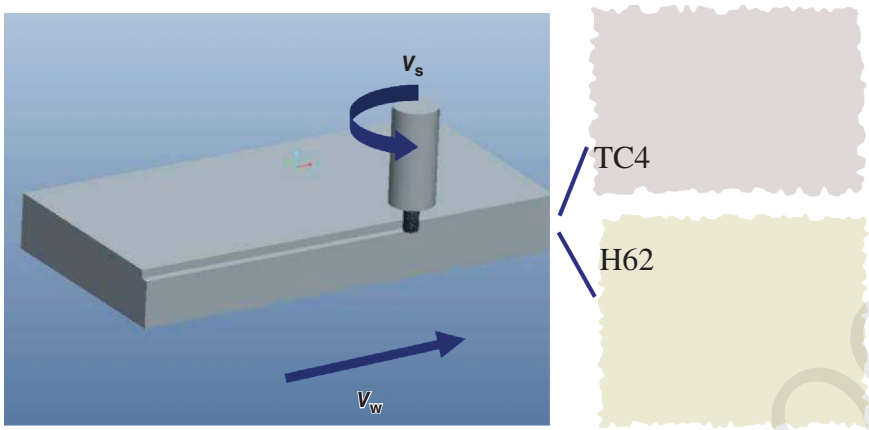

Figure 1.19 Micro numerical control machine, micro-grinding tool, and micro-manufacturing feature of Northeastern University.

Experiments on quartz glass showed that ultrasonic assistance significantly reduced grinding forces and enabled ductile-mode machining, improving surface quality. Moreover, the decrease in grinding forces expanded the range of grinding parameters, allowing the use of larger parameters to enhance processing efficiency.

Lubrication is crucial in grinding as it reduces friction, lowers processing temperatures, and improves both grinding performance and abrasive lifespan.

Dull abrasives significantly reduce grinding performance. While dressing dull grinding wheels is relatively easy in conventional grinding, the small size and fine abrasives of micro-grinding tools make dressing more challenging. Feng et al. [17] investigated the micro-grinding of ceramic end-faces and examined how tool wear and stiffness affect grinding forces, system vibration, acoustic emission signals, and spindle load. They introduced a tool-wear monitoring approach that combines grinding force and system vibration signals and validated its feasibility under various processing conditions. Although the study focused on ceramics, challenges remain due to the low stiffness of micro-tools and the high grinding forces required for hard, brittle materials.

Gong et al. [14] developed a micro-grinding machine and produced micro-feature components, as shown in Figure 1.19, while analyzing how different parameters affect the surface quality of TC4 and H62 in micro-grinding.

1.5 Contents of this book

The main contents of this book are as follows:

Part I: A brief description of grinding technology (including conventional and micro-grinding) for single-crystal nickel alloys is provided. Particularly, the development of understanding in grinding mechanisms, grinding characteristics, grinding process simulation, and control for single-crystal nickel alloys is analyzed, and some crucial issues in high-efficiency and high-quality grinding

of single-crystal nickel alloys are provided and need more attention. In addition, the grinding mechanism of single-crystal nickel alloy, both in conventional and micro-grinding, is presented by means of FEM and theoretical analysis. These contents provide a foundation for an in-depth understanding of the following analysis on the grindability of single-crystal nickel alloy.

Part II: This section evaluates the grinding characteristics of single-crystal nickel alloys comparatively and comprehensively, in terms of grinding force, temperature, and grinding wheel wear behavior in both conventional and micro-grinding processes. The massive data on such aspects is valuable and could be used for optimization and further control of single-crystal nickel alloy grinding.

Part III: The surface integrity of single-crystal nickel alloy in conventional grinding (i.e., surface grinding and profile grinding) is examined both at micro- and nano-scales. Many indicators of surface integrity, such as grinding surface topography, surface roughness, microhardness, subsurface microstructure, residual stresses, and even fretting behavior, are assessed in detail.

Part IV: The micro-grinding-induced surface integrity of single-crystal nickel alloy is studied. In particular, the effects of micro-grinding parameters on surface integrity indicators (i.e., surface roughness, surface topography, subsurface damage, recrystallization, and so on) are analyzed comprehensively and deeply.

Part V: This section develops the simulation and theoretical models for predicting the grinding temperature and residual stresses in profile grinding of single-crystal nickel alloy components. The obtained results agree well with the experimental ones, indicating the feasibility of the present models to be used for optimization and controlling the grinding process of the single-crystal nickel alloy component with complex shape/structure.

References

1 Grimmert, A., Florian, P., and Petra, W. (2023). Temperature modeling of creep-feed grinding processes for nickel-based superalloys with variable heat flux distribution. *CIRP Journal of Manufacturing Science and Technology* 41: 477–489.

2 Ding, W.F., Miao, Q., Li, B.K. et al. (2019). Review on grinding technology of nickel-based superalloys used for aero-engine. *Journal of Mechanical Engineering* 55: 189–215.

3 Das, N. (2010). Advances in nickel-based cast superalloys. *Transactions of the Indian Institute of Metals* 63: 265–274.

4 Liang, C., Gong, Y., Li, P. et al. (2023). Subsurface deformation and burr formation in nickel-based single-crystal superalloy under grinding. *Archives of Civil and Mechanical Engineering* 23: 126.

5 Sun, Y., Jin, L., Gong, Y. et al. (2022). Experimental evaluation of surface generation and force time-varying characteristics of curvilinear grooved micro end mills fabricated by EDM. *Journal of Manufacturing Processes* 73: 799–814.

6 Parrott, E. (1983). Development and application of continuous dress creep feed grinding. *Proceedings of the Institution of Mechanical Engineers, Part B: Management and engineering manufacture* 197 (4): 231–235.

7 Gu, Y., Li, H., Du, B. et al. (2019). Towards the understanding of creep-feed deep grinding of DD6 nickel-based single-crystal superalloy. *The International Journal of Advanced Manufacturing Technology* 100: 445–455.

8 Meira, F., Renato, P., and Jose, C.P. (2020). Optimization of creep feed grinding using CBN wheels on nickel-based superalloys: a case study. *Journal of Manufacturing Technology Research* 12: 1–17.

9 Cai, M., Zhu, T., Gao, X. et al. (2022). Study on machining performance in grinding of Ni-base single crystal superalloy DD5. *The International Journal of Advanced Manufacturing Technology* 120 (11): 7657–7671.

10 Yao, C., Luo, J., Tan, L. et al. (2023). Experimental investigation on surface integrity and fatigue of nickel-based single-crystal superalloy DD6 during grinding-shot peening composite manufacturing. *The International Journal of Advanced Manufacturing Technology* 125 (7): 3449–3463.

11 Zhang, W., Gong, Y., Zhao, X. et al. (2023). Modeling and analysis of tangential force in robot abrasive belt grinding of nickel-based superalloy. *Archives of Civil and Mechanical Engineering* 23: 124.

12 Zhao, B., You, H., Miao. Q. et al. (2025). Surface integrity characterization of third-generation nickel-based single crystal blade tenons after ultrasonic vibration-assisted grinding. *Chinese Journal of Aeronautics* 38: 103138.

13 Miao, Q., Ding, W., Gu, Y. et al. (2019). Comparative investigation on wear behavior of brown alumina and microcrystalline alumina abrasive wheels during creep feed grinding of different nickel-based superalloys. *Wear* 426: 1624–1634.

14 Xu, Y., Gong, Y., Zhang, W. et al. (2022). Microstructure evolution and dynamic recrystallization mechanism induced by grinding of Ni-based single crystal superalloy. *Journal of Materials Processing Technology* 310: 117784.

15 Li, J., Xiong, D., Zhang, Y. et al. (2011). Friction and wear properties of MoS2-overcoated laser surface-textured silver-containing nickel-based alloy at elevated temperatures. *Tribology Letters* 43: 221–228.

16 Chen, W., Sun, Y., Feng, X. et al. (2023). Atomic-scale study of linear reciprocating friction of TCP/γ phase in nickel-based single crystal alloy. *Physica Scripta* 98: 125021.

17 Feng, X., Zhu, Z., Wu, Z. et al. (2023). Atomic-scale study of the repeated friction processes of γ/γ' phase nickel-based single crystal alloys. *Tribology International* 185: 108538.

18 Zhang, M., Cai, M., Gong, Y. et al. (2024). Experimental study on the effect of minimum quantity lubrication on the grinding surface/subsurface of nickel-based single-crystal superalloys. *The International Journal of Advanced Manufacturing Technology* 134: 5375–5390.

19 Guo, C., Campomanes, M., Mcintosh, D. et al. (2003). Optimization of continuous dress creep-feed form grinding process. *CIRP Annals* 52 (1): 259–262.

20 You, H., Zhao, B., Ding, W. et al. (2024). Wear behavior of white alumina and seeded gel abrasive wheels in ultrasonic vibration-assisted grinding of nickel-based single-crystal alloy. *Wear* 556: 205505.

21 Jin, Q., Cao, S., Wang, W. et al. (2022). Study on surface integrity of DD5 nickel-based single crystal super-alloy in creep-feed grinding. *Xibei Gongye Daxue Xuebao/Journal of Northwestern Polytechnical University* 40 (1): 189–198.

22 Jin, Q., Liu, H., Zhang, S. et al. (2022). Experimental study on grinding surface quality of DD9 nickel-based single crystal super-alloy. *Advances in Aeronautical Science and Engineering* 14 (1): 73–80.

23 Gong, Y.D., Zhou, J., Zhou, Y.G. et al. (2018). Micro-grinding temperature simulation for nickel-based single crystal superalloy. *Journal of Northeastern University (Natural Science)* 39: 82.

24 Zhou, Y., Ma, L., Gong, Y. et al. (2019). Study on force and temperature characteristics of micro-grinding nickel-based single-crystal superalloy. *Journal of the Brazilian Society of Mechanical Sciences and Engineering* 41: 1–18.

25 Ding, Q., Lao, Z., Wei, H. et al. (2020). Site occupancy of alloying elements in γ' phase of nickel-base single crystal superalloys. *Intermetallics* 121: 106772.

26 Wang, C., Yan, X., Liao, H. et al. (2021). Process parameter optimization and anisotropy sensitivity study for abrasive belt grinding of nickel-based single-crystal superalloy. *Archives of Civil and Mechanical Engineering* 21: 1–18.

27 Miao, Q., Ding, W., Kuang, W. et al. (2022). Microstructure evolution and formation of gradient structures in single crystal nickel-based superalloy by surface mechanical creep-feed grinding treatment. *Materials* 16: 321.

28 Miao, Q., Ding, W., Xu, J. et al. (2021). Creep feed grinding induced gradient microstructures in the superficial layer of turbine blade root of single crystal nickel-based superalloy. *International Journal of Extreme Manufacturing* 3: 045102.

29 Miao, Q., Ding, W., Kuang, W. et al. (2022). Indentation behavior of creep-feed grinding induced gradient microstructures in single crystal nickel-based superalloy. *Materials Letters* 306: 130956.

30 Qian, N., Jamil, M., Ding, W. et al. (2024). Thermal management in grinding of superalloys–A critical review. *Journal of Intelligent Manufacturing and Special Equipment* 5: 3–33.

31 Ge, Y., Zhu, Z., and Zhu, Y. (2019). Electrochemical deep grinding of cast nickel-base superalloys. *Journal of Manufacturing Processes* 47: 291–296.

32 Zhou, Y., Wen, X., Yin, G. et al. (2021). Study on theoretical model of roughness and wear of the microgrinding tool in microgrinding nickel-based single crystal superalloy. *Journal of the Brazilian Society of Mechanical Sciences and Engineering* 43: 317.

33 Gong, Y., Li, Q., Li, J. et al. (2018). Tool wear performance and surface integrity studies for milling DD5 Ni-based single crystal superalloy. *Science China Technological Sciences* 61: 522–534.

34 Huang, M. and Jing, Z. (2016). An overview of rhenium effect in single-crystal superalloys. *Rare Metals* 35 (2): 127–139.

35 Gong, Y., Zhou, Y., Wen, X. et al. (2017). Experimental study on micro-grinding force and subsurface microstructure of nickel-based single crystal superalloy in micro grinding. *Journal of Mechanical Science and Technology* 31: 3397–3410.

36 Park, K.H. and Paul, W. (2018). Observation of the dissolution of topologically close packed phases by an additional heat treatment in third generation nickel-based single crystal superalloy turbine blades. *Advanced Engineering Materials* 20: 1700987.